TABLE I
ANALYTICAL VALUES AND EXPERIMENTAL RESULTS (IN PARENTHSES) WITH RESPECT TO k AND C_Δ FOR STRATEGY A AND STRATEGY B

		pf		DC current required (mA)		$I_{L2,rms}$ (mA)
		A	B	A	B	B
k = 0.04 (A/V)	C_Δ = 0.05	0.994 (0.990)	0.994 (0.988)	25 (27)	25 (28)	11.8 (13)
	C_Δ = 0.1	0.994 (0.987)	0.994 (0.983)	50 (54)	50 (54)	23.6 (27)
	C_Δ = 0.2	0.993 (0.985)	0.993 (0.981)	100 (103)	100 (105)	47.1 (55)
C_Δ = 0.1	k = 0.04	0.994 (0.987)	0.994 (0.983)	50 (54)	50 (54)	23.6 (27)
	k = 0.07	0.983 (0.975)	0.983 (0.977)	50 (54)	50 (53)	23.6 (28)
	k = 0.1	0.934 (0.940)	0.934 (0.928)	50 (53)	50 (54)	23.6 (27)

and experimental results with respect to k and C_Δ for strategy A and strategy B. We can conclude that C_Δ and I_0/I_L influence the power factor far less than k does. This can be explained from the results shown in Table I, that the dc current required $(C_\Delta I_o)$ to eliminate the voltage imbalance is usually much smaller than I_L. Also, the even harmonics introduced in strategy B is negligible when using a larger k.

V. CONCLUSION

The voltage imbalance in the split capacitors is a disadvantage of the half-bridge boost rectifier. In this letter, the imbalance phenomenon and the method of overcoming it have been discussed in detail. It is proved that the optimal compensation scheme is to add only a required dc component in the source current.

REFERENCES

[1] J. T. Boys and A. W. Green, "Current-forced single phase reversible rectifier," *Proc. Inst. Elect. Eng.*, pt. B, vol. 136, no. 5, pp. 205–211, 1989.
[2] R. Srinivasan and R. Oruganti, "A unity power factor converter using half-bridge boost topology," *IEEE Trans. Power Electron.*, vol. 13, pp. 487–499, May 1998.
[3] J. C. Salmon, "Circuit topologies for single-phase voltage-doubler boost rectifier," *IEEE Trans. Power Electron.*, vol. 8, pp. 521–529, July 1993.

Design and Implementation of a New Sliding-Mode Observer for Speed-Sensorless Control of Induction Machine

Adnan Derdiyok, Mustafa K. Güven, Habib-ur Rehman, Nihat Inanc, and Longya Xu

***Abstract*—In this letter, a new sliding-mode sensorless control algorithm is proposed for the field-oriented induction machine drive. In the proposed algorithm, the terms containing flux, speed, and rotor time constant, which are common in both current and flux equations, in the current model of the induction machine are estimated by a sliding function. The flux and speed estimation accuracy is guaranteed when the error between the actual current and observed current converges to zero. Hence, the fourth-order system is reduced to two second-order systems, and the speed estimation becomes very simple and robust to the parameter uncertainties. The new approach is verified by simulation and experimental results.**

***Index Terms*—Induction motor, field-oriented control, sensorless control, sliding mode.**

I. INTRODUCTION

A traditional rotor-flux-oriented induction machine drive offers control performance but often requires additional sensors on the machine. This adds to the cost and complexity of the drive system. To avoid using sensors on the machine, terminal quantities of the machine are used to estimate the flux and speed of the machine. For the last two decades, many researchers attempted to solve this problem, and for this purpose, different algorithms have been proposed [1]–[11].

For this problem, sliding mode is rarely used, even though sliding-mode theory is one of the prospective control methodologies for induction machine flux and speed estimation problems because of its order reduction, disturbance rejection, robustness, and simplicity of implementation. The basics of the sliding-mode control for electromechanical systems are introduced in [12]. A few works have been presented for the speed and flux estimation for the induction machine using sliding-mode theory [13], [14].

In this letter, a new sliding-mode-based flux and speed estimation technique for sensorless control of a field-oriented induction machine is proposed. The flux estimation accuracy is guaranteed through the current observer. The rotor speed is estimated based on the measured and estimated stator currents and estimated rotor flux. The proposed algorithm estimates the rotor time constant along with the rotor speed, and problems related to integration process are solved through a low-pass filter structure. In the proposed algorithm the terms containing flux, speed, and rotor time constant, which are common in both current and flux equations of the current model of the induction machine, are estimated by a sliding function. This makes d- and q-axes flux estimation decoupled and, therefore, the flux estimation is merely an integration of the known terms.

II. THEORETICAL ASPECTS

In this section, the induction machine model and the theoretical aspects of the proposed algorithm are introduced, including current observer, flux, speed, and rotor time constant estimation.

Manuscript received September 15, 2000; revised June 12, 2002. Abstract published on the Internet July 15, 2002.

A. Derdiyok, H. Rehman, N. Inanc, and L. Xu are with the Department of Electrical Engineering, The Ohio State University, Columbus, OH 43210 USA.
M. K. Güven is with Technical Center E-855, Caterpillar Inc., Peoria, IL 61656-1875 USA.

Publisher Item Identifier 10.1109/TIE.2002.803247.

A. Induction Machine Model

The induction machine model is defined by the stator currents and rotor fluxes as state variables in the rotor-flux-oriented stationary reference frame by the following equations:

$$\begin{aligned}\frac{\partial i_{ds}^s}{\partial t} =&\beta\frac{1}{T_r}\lambda_{dr}^s + \beta\omega_r\lambda_{qr}^s - k_1 i_{ds}^s + k_2 V_{ds}^s\\ \frac{\partial i_{qs}^s}{\partial t} =&\beta\frac{1}{T_r}\lambda_{qr}^s - \beta\omega_r\lambda_{dr}^s - k_1 i_{qs}^s + k_2 V_{qs}^s\\ \frac{\partial \lambda_{dr}^s}{\partial t} =&-\frac{1}{T_r}\lambda_{dr}^s - \omega_r\lambda_{qr}^s + \frac{L_m}{T_r} i_{ds}^s\\ \frac{\partial \lambda_{qr}^s}{\partial t} =&-\frac{1}{T_r}\lambda_{qr}^s + \omega_r\lambda_{dr}^s + \frac{L_m}{T_r} i_{qs}^s\end{aligned} \tag{1}$$

where

$$\begin{aligned}\sigma =&1 - \frac{L_m^2}{L_s L_r}\\ T_r =&\frac{L_r}{R_r}\\ k_2 =&\frac{1}{\sigma L_s}\\ \beta =&\frac{k_2 L_m}{L_r}\\ k_1 =&k_2\left(R_S + \frac{L_m^2}{L_r T_r}\right).\end{aligned}$$

T_r is the rotor time constant, ω_r is the rotor electrical speed, subscripts d and q are used for d-axis and q-axis components, and superscript s represents the stationary reference frame. L_m, L_r, R_r, L_s, and R_s are mutual inductance, rotor inductance and resistance, and stator inductance and resistance, respectively.

B. Current Observer Design

The proposed speed and rotor time constant estimation structures are based on a sliding-mode current observer. Ensuring the convergence of the current observer, the equivalent control [15] is produced. Then, it is used in the flux estimation to determine the flux along d and q axes. Finally, the rotor speed and rotor time constant are estimated by using estimated flux and the sliding function. For clarity, let (1) be written as

$$\begin{aligned}\dot{\mathbf{I}} =&\beta\mathbf{A}\mathbf{\Lambda} - k_1\mathbf{I} + k_2\mathbf{V}\\ \dot{\mathbf{\Lambda}} =&-\mathbf{A}\mathbf{\Lambda} + \frac{L_m}{T_r}\mathbf{I}\end{aligned} \tag{2}$$

where

$$\begin{aligned}\dot{\mathbf{I}} =&\left[\frac{\partial i_{ds}^s}{\partial t}, \frac{\partial i_{qs}^s}{\partial t}\right]^T\\ \dot{\mathbf{\Lambda}} =&\left[\frac{\partial \lambda_{dr}^s}{\partial t}, \frac{\partial \lambda_{qr}^s}{\partial t}\right]^T\\ \mathbf{I} =&\left[i_{ds}^s, i_{qs}^s\right]^T\\ \mathbf{\Lambda} =&\left[\lambda_{dr}^s, \lambda_{qr}^s\right]^T\\ \mathbf{A} =&\begin{bmatrix}\frac{1}{T_r} & \omega_r\\ -\omega_r & \frac{1}{T_r}\end{bmatrix}\\ \mathbf{V} =&\left[V_{ds}^s, V_{qs}^s\right]^T.\end{aligned}$$

Based on the model given in (2), the proposed current observer structure is

$$\dot{\hat{\mathbf{I}}} = \beta\mathbf{\Psi} - k_1\hat{\mathbf{I}} + k_2\mathbf{V} \tag{3}$$

where

$$\begin{aligned}\dot{\hat{\mathbf{I}}} =&\left[\frac{\partial \hat{i}_{ds}^s}{\partial t}, \frac{\partial \hat{i}_{qs}^s}{\partial t}\right]^T\\ \hat{\mathbf{I}} =&\left[\hat{i}_{ds}^s, \hat{i}_{qs}^s\right]^T\\ \mathbf{\Psi} =&[\Psi_d, \Psi_q]^T\\ \mathbf{V} =&\left[V_{ds}^s, V_{qs}^s\right]^T.\end{aligned}$$

$\hat{i}_{ds}^s$ and $\hat{i}_{qs}^s$ are the observed stator current components in the stationary reference frame. The sliding functions Ψ_d and Ψ_q are defined as

$$\begin{aligned}\Psi_d =&-u_o\mathrm{sign}(s_d)\\ \Psi_q =&-u_o\mathrm{sign}(s_q)\end{aligned} \tag{4}$$

where

$$\begin{aligned}s_d =&\hat{i}_{ds}^s - i_{ds}^s\\ s_q =&\hat{i}_{qs}^s - i_{qs}^s\end{aligned} \tag{5}$$

and

$$\mathrm{sign}(s_{dq}) = \begin{cases}1, & \text{if } s_{dq} > 0\\ -1, & \text{if } s_{dq} < 0\end{cases}$$

and the sliding mode surface is defined as

$$s_n = [\,s_{ds} \quad s_{qs}\,]^T. \tag{6}$$

When the estimation error trajectories reach the sliding surface, i.e., $s_n = 0$, then, from (5), it is obvious that observed current will converge to the actual ones, i.e., $\hat{i}_{ds}^s = i_{ds}^s$ and $\hat{i}_{qs}^s = i_{qs}^s$. It is important to point out that this sliding surface equation selection guarantees that on the sliding surface the observer will not be aeffected by any system parameter or any disturbance, i.e., the current observer is invariant [15].

Claim: Consider the sliding surface $s_n = [\,s_d, s_q\,]^T$ defined by (5), and the discontinuous control law $\mathbf{\Psi}$ defined by (4), and if

$$u_o > \frac{\left|\bar{\mathbf{I}}^T\mathbf{A}\mathbf{\Lambda}\right| - \frac{k_1}{q}\bar{\mathbf{I}}^T\bar{\mathbf{I}}}{\left|\bar{i}_{ds}^s\right| + \left|\bar{i}_{qs}^s\right|}$$

where

$$\bar{i}_{ds}^s = \hat{i}_{ds}^s - i_{ds}^s \quad \bar{i}_{qs}^s = \hat{i}_{qs}^s - i_{qs}^s$$

then, sliding surface s_n is attractive.

Proof: Let us consider the Lyapunov function $V = 0.5 s_n^T s_n$, where its time derivative is $\dot{V} = s_n^T\dot{s}_n$.

Then, using (2) and (3) $\dot{s}_n$ can be written as

$$\dot{s}_n = \dot{\bar{\mathbf{I}}} = q\,(\mathbf{\Psi} - \mathbf{A}\mathbf{\Lambda}) - k_1\bar{\mathbf{I}}.$$

The sliding-mode surface is attractive if $\dot{V} = s_n^T\dot{s}_n < 0$, i.e.,

$$q\bar{\mathbf{I}}^T\left(-u_o\mathrm{Sign}(\bar{\mathbf{I}}) - \mathbf{A}\mathbf{\Lambda}\right) - k_1\bar{\mathbf{I}}^T\bar{\mathbf{I}} < 0$$

that is,

$$u_o > \frac{\left|\bar{\mathbf{I}}^T\mathbf{A}\mathbf{\Lambda}\right| - \frac{k_1}{q}\bar{\mathbf{I}}^T\bar{\mathbf{I}}}{\left|\bar{i}_{ds}^s\right| + \left|\bar{i}_{qs}^s\right|}. \tag{7}$$

By selecting large enough u_o, found by the existence condition given by (7), the sliding mode $(s_n = 0)$ will occur. To define the control action, which maintains the motion on the sliding manifold, "equivalent control" concept is introduced [15]. The equivalent control can be defined as the average of the discontinuous control on the sliding manifold, which by itself is sufficient to maintain the motion on the manifold. Therefore, the equivalent control action can be found by isolating the continuous term using a low-pass filter, which is implemented as

$$\Psi_{dq}^{eq} = \frac{1}{\mu s + 1}\Psi_{dq}$$

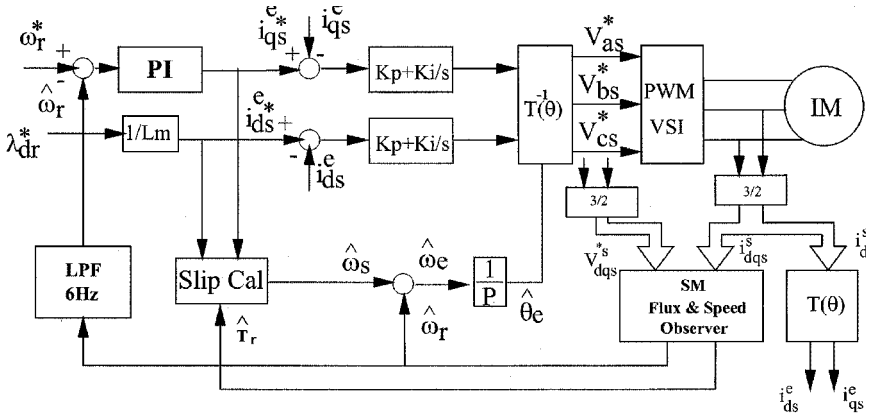

Fig. 1. Block diagram of the simulation and implementation of IFO control induction machine drive system.

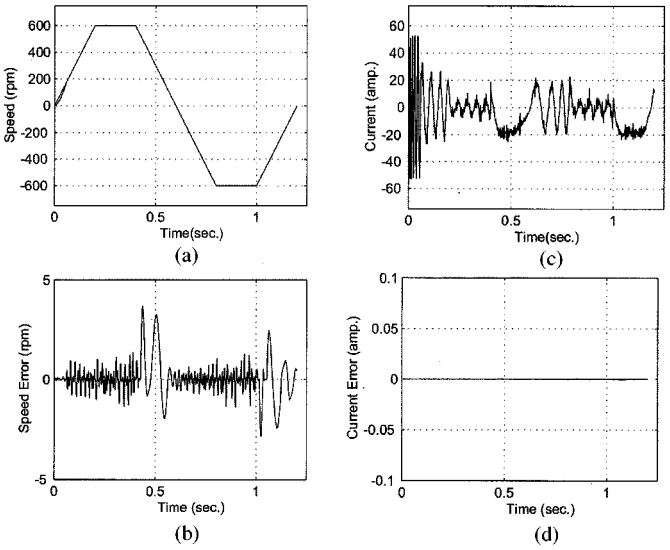

Fig. 2. (a) Actual and estimated speeds, (b) the speed error, (c) observed and actual currents, and (d) error between them for trapezoidal reference.

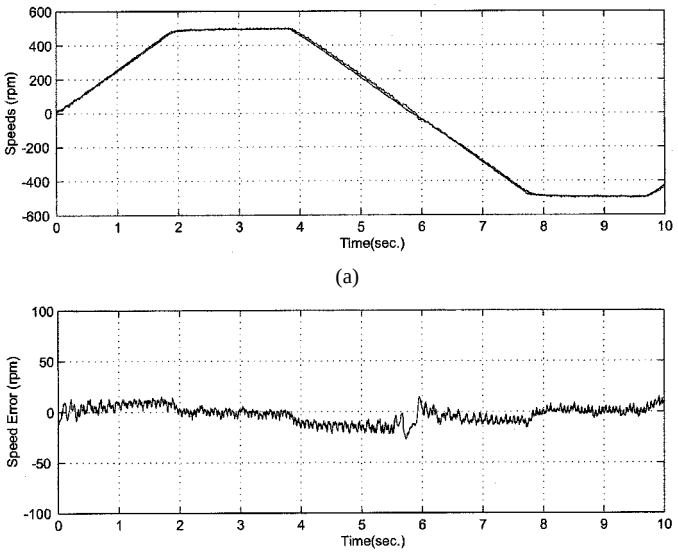

Fig. 3. (a) Actual and estimated speeds and (b) speed error between them.

where μ is the time constant of the filter and should be sufficiently small to preserve the slow component undistorted but large enough to eliminate the high-frequency components.

C. Flux, Speed, and Rotor Time Constant Estimation

When the trajectories of the system reach the sliding surface $s_n = 0$, the observed currents $\hat{i}^s_{qs}$ and $\hat{i}^s_{ds}$ match with the actual currents i^s_{qs} and i^s_{ds}, which means the sliding function will represent the term that is replaced by them, i.e.,

$$\mathbf{\Psi} = \mathbf{A}\mathbf{\Lambda}. \tag{8}$$

When this is substituted in (2), then

$$\begin{bmatrix} \frac{\partial \lambda^s_{dr}}{\partial t} \\ \frac{\partial \lambda^s_{qr}}{\partial t} \end{bmatrix} = -\begin{bmatrix} \Psi^{eq}_d \\ \Psi^{eq}_q \end{bmatrix} + \frac{1}{T_r} L_m \begin{bmatrix} i^s_{ds} \\ i^s_{qs} \end{bmatrix}$$

from which the rotor flux λ^s_{dr} and λ^s_{qr} can be found. Note that to calculate the fluxes, a low-pass filter is used instead of integration. Note that this approach was introduced in [15] and showed that it overcomes the problems of an ideal integration such as the effect of initial conditions. Now, using the flux values and (8), speed and rotor time constant can be found. For this, let (8) be written as

$$\begin{bmatrix} \Psi^{eq}_d \\ \Psi^{eq}_q \end{bmatrix} = \begin{bmatrix} \frac{1}{T_r} & \omega_r \\ -\omega_r & \frac{1}{T_r} \end{bmatrix} \begin{bmatrix} \lambda^s_{dr} \\ \lambda^s_{qr} \end{bmatrix}$$

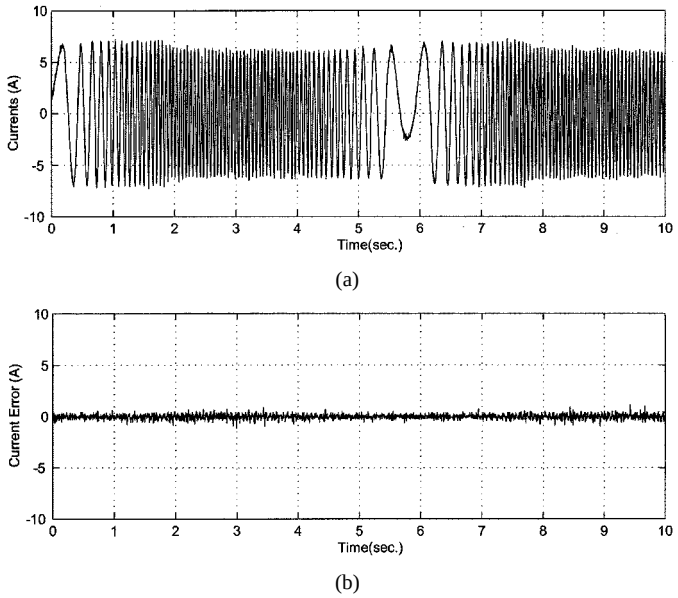

Fig. 4. (a) Actual and observed d-axis currents and (b) current error between them.

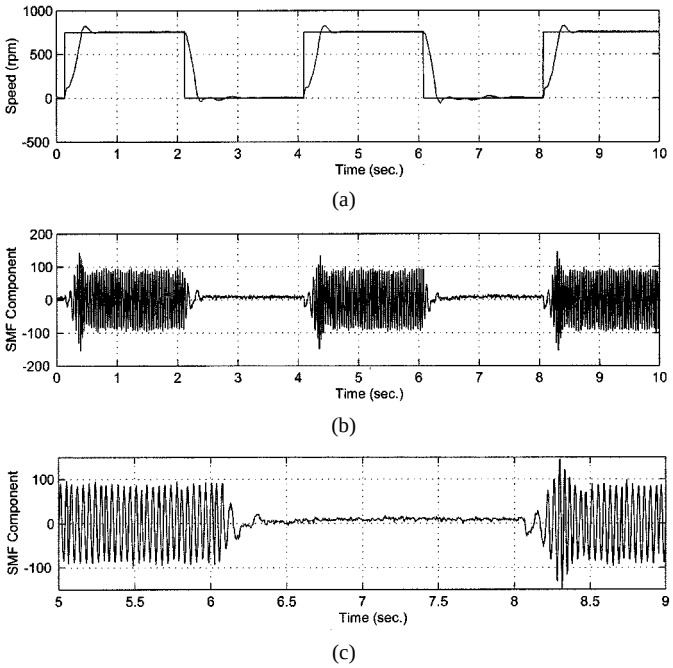

Fig. 5. (a) Actual and estimated speeds, (b) sliding function d-component, and (c) the same sliding function component zoomed.

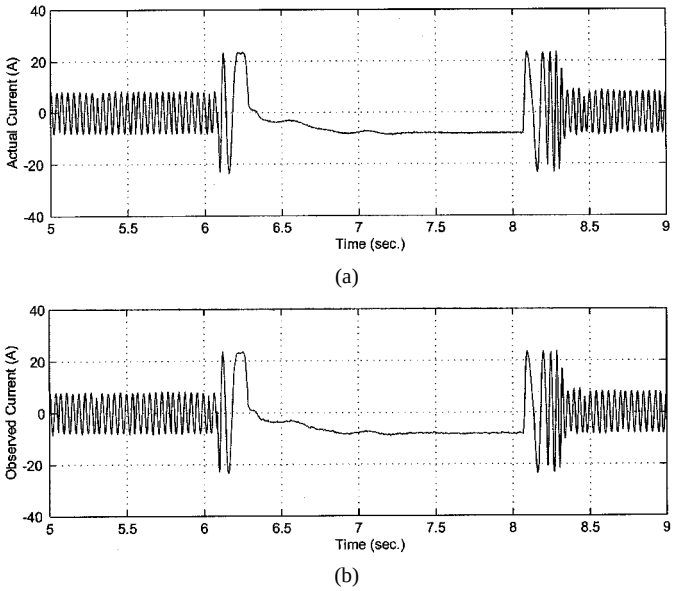

Fig. 6. (a) Actual d-axis current and (b) observed d-axis current.

which can be reorganized as

$$\begin{bmatrix} \Psi_d^{eq} \\ \Psi_q^{eq} \end{bmatrix} = \begin{bmatrix} \lambda_{dr}^s & \lambda_{qr}^s \\ \lambda_{qr}^s & -\lambda_{dr}^s \end{bmatrix} \begin{bmatrix} \frac{1}{T_r} \\ \omega_r \end{bmatrix}$$

and

$$\begin{bmatrix} \frac{1}{T_r} \\ \omega_r \end{bmatrix} = \frac{1}{|\lambda_r|} \begin{bmatrix} -\lambda_{dr}^s & -\lambda_{qr}^s \\ -\lambda_{qr}^s & \lambda_{dr}^s \end{bmatrix} \begin{bmatrix} \Psi_d^{eq} \\ \Psi_q^{eq} \end{bmatrix} \tag{9}$$

where

$$|\lambda_r| = -(\lambda_{dr}^s)^2 - (\lambda_{qr}^s)^2.$$

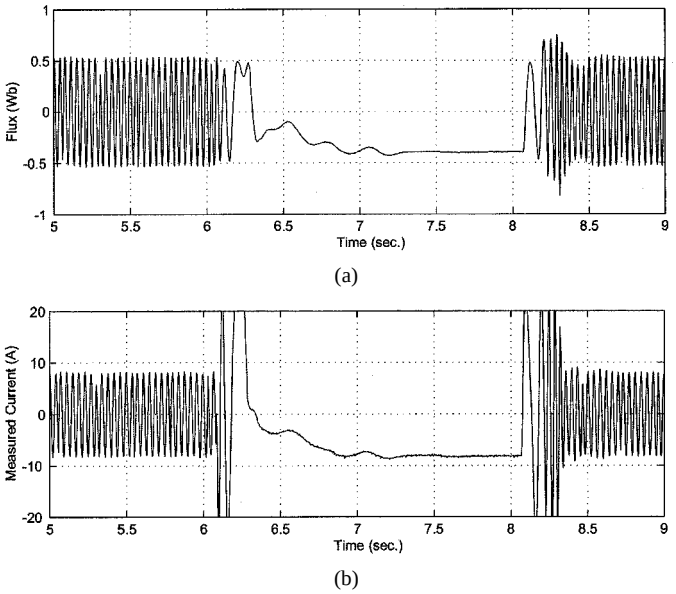

Fig. 7. (a) d-axis flux component and (b) measured phase current.

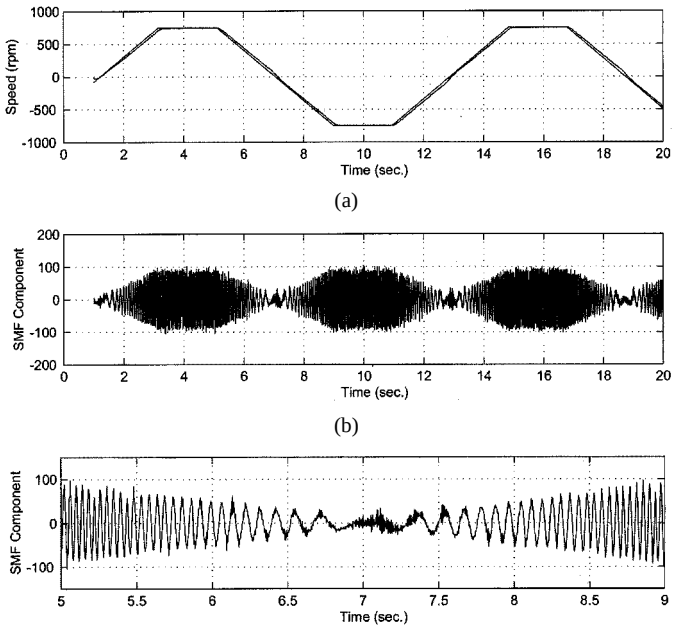

Fig. 8. (a) Actual and observed speeds, (b) sliding function d-component, and (c) the same sliding function component zoomed.

Finally, from (9), ω_r and $1/T_r$ are found as

$$\omega_r = \frac{1}{|\lambda_r|}\left(\lambda_{dr}^s \Psi_q^{eq} - \lambda_{qr}^s \Psi_d^{eq}\right)$$
$$\frac{1}{T_r} = -\frac{1}{|\lambda_r|}\left(\lambda_{dr}^s \Psi_d^{eq} + \lambda_{qr}^s \Psi_q^{eq}\right).$$

III. Simulation and Experimental Studies

In this section, the performance of the proposed observer structure is presented via simulation and experimental results. The block diagram of the indirect field-oriented induction machine drive system with observer structure is given in Fig. 1. In the speed regulation loop, a simple proportional-plus-integral (PI) controller is used. It is assumed that the

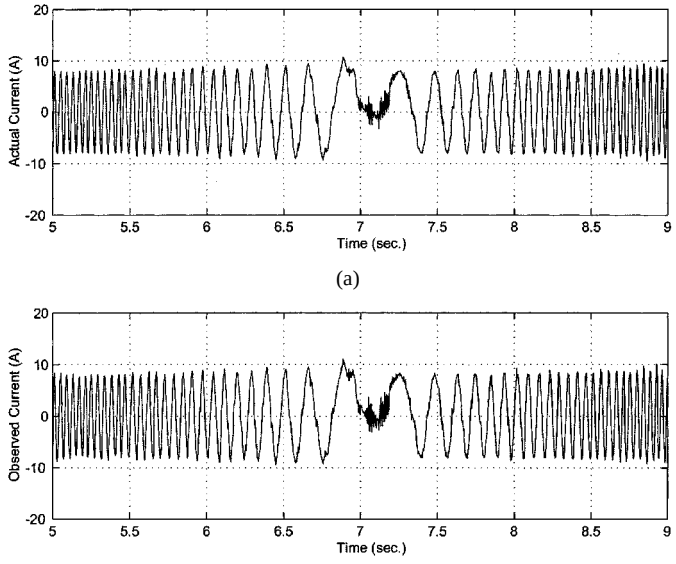

Fig. 9. (a) Actual d-axis current and (b) observed d-axis current.

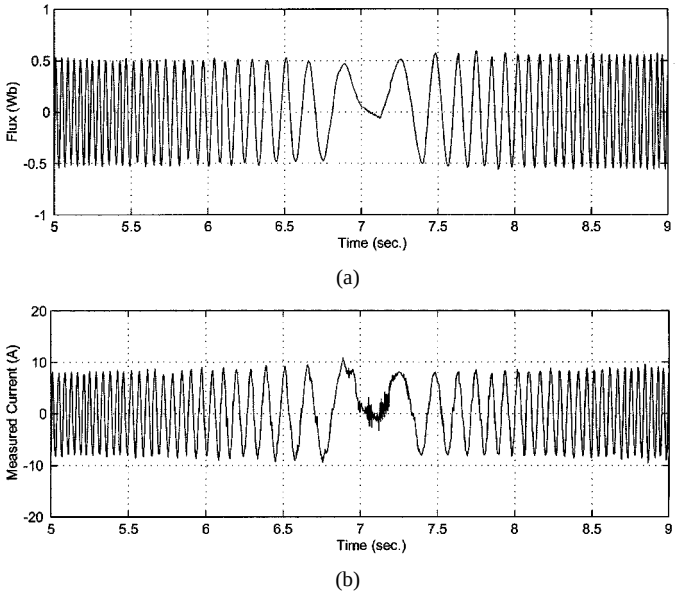

Fig. 10. (a) d-axis flux component and (b) measured phase current.

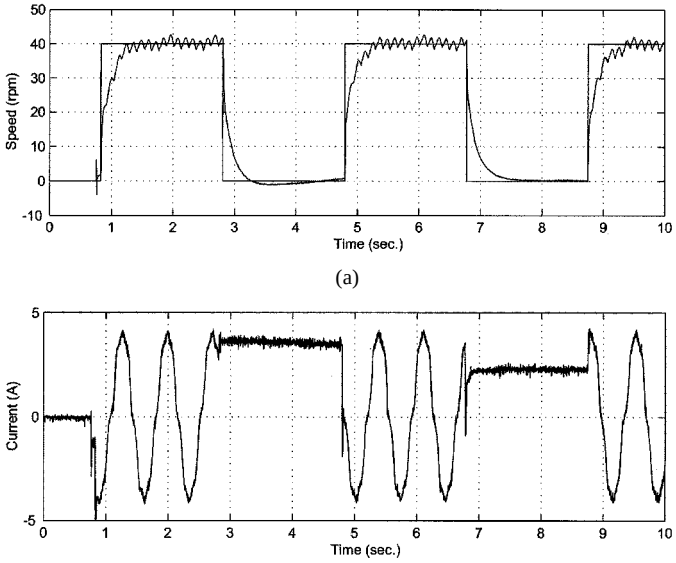

Fig. 11. (a) Command and observed speeds and (b) observed and measured d axis currents.

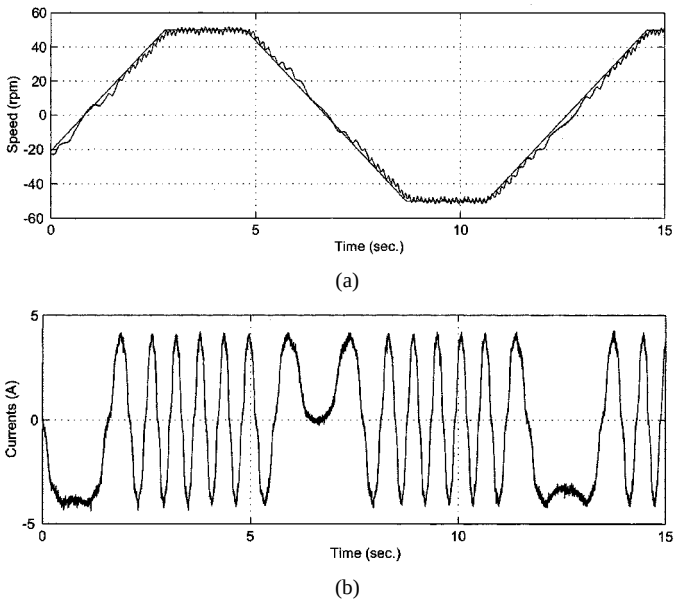

Fig. 12. (a) Command and observed speeds and (b) observed and measured d axis currents.

performance of the PI controller will be sufficient to present the performance of the observer structure. It is important to point out that the rotor time constant estimation is also presented. Note that a four-pole 5-hp induction machine was used in this study, the parameters of which are $L_{ls} = L_{lr} = 1.9$ mH, $L_m = 41.2$ mH, $R_s = 0.6$, and $R_r = 0.412$.

A. Simulation Results

The validity of the observer structure is verified by the simulation, and the results are given in Fig. 2, where the estimated speed is used as feedback in the closed loop. The first step for the speed estimation is the current observation. The observed and actual d–axis currents are shown in Fig. 2(c), and the error between them is given in Fig. 2(d). It is obvious from these results that current convergence is satisfied.

B. Experimental Results

The laboratory setup consists of a 5-hp cage rotor induction machine and a high-performance advance controller for electric machines (ACE). The ACE is a very-high-performance, rugged, rapid prototyping tool that implements advanced control algorithms and interfaces without any traditional programming. It is important to note that all the experimental results presented in this paper have been collected using the data acquisition capability of the ACE controller. The performance of the observer is first analyzed in the implementation by operating the observer without using it in the closed loop, i.e., in the feedback, the actual speed from the encoder is used and the observer structure works parallel to the overall system without affecting the closed-loop system at all. This will be called "free operation." For this case, the closed-loop system follows a trapezoidal trajectory, and parallel with the closed-loop system, the observer operates and estimates the encoder speed. The estimated speed and encoder output are given in Fig. 3(a) together with the error between them in Fig. 3(b). In addition, observed and measured currents for the d axis, and the error between them, are given in Fig. 4. These results verify the

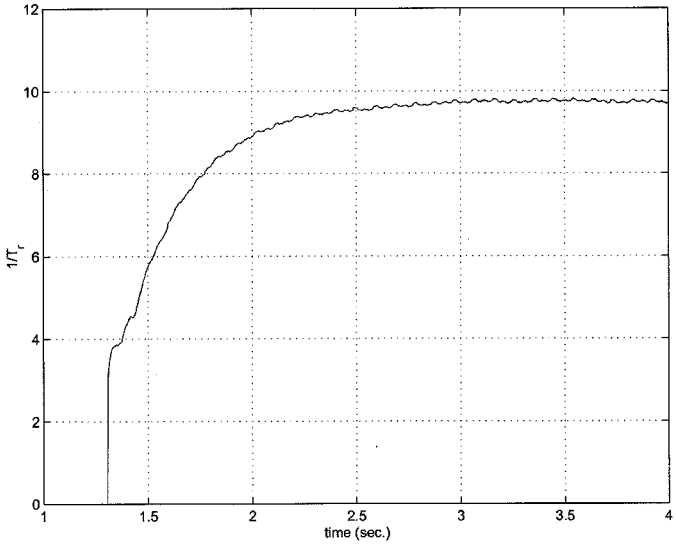

Fig. 13. Estimation of $1/T_r$ for induction machine used.

performance of the observer. Next, the observer is tested when it is replaced with the encoder in the closed loop, which is called "feedback operation" of the observer. For high-speed performance, a 750-r/min square and trapezoidal reference inputs are applied to the closed-loop system. In addition, for the low-speed performance, a 40-r/min square and a 50-r/min trapezoidal reference input are applied. In the following cited figures, these results are presented. Specifically, in Figs. 5–10, observed and command speeds, sliding function, actual and observed d-axis currents, observed flux, and measured phase current are shown for high speeds. In Figs. 11(a) and 12(a), the observed and command speeds, and in Figs. 11(b) and 12(b), observed and measured d-axis currents are presented. It is important to point out that the observed and measured currents are on top of each other. In addition, the rotor time constant is updated and, as seen from Fig. 13, it converges to its actual value in a short period of time.

IV. Concluding Remarks

A new sliding-mode current observer has been proposed for flux, speed, and rotor time constant estimations. The rotor time constant update algorithm will overcome the problem of rotor resistance variation, normally needed for the slip frequency control in indirect field-oriented vector control. The proposed scheme is validated through simulation and experimental results. It is concluded from the results presented in this letter that the proposed scheme performs well for both high and low speed. It is also important that the new algorithm is robust to parameter changes and easy to implement for an off-the-shelf machine.s

References

[1] P. Jansen and R. Lorenz, "A physically insightful approach to the design and accuracy assessment of flux observers for field oriented induction machine drives," *IEEE Trans. Ind. Applicat.*, vol. 30, pp. 101–110, Jan./Feb. 1994.

[2] C. Schauder, "Adaptive speed identification for vector control of induction motors without rotational transducers," in *Conf. Rec. IEEE-IAS Annu. Meeting*, 1989, pp. 493–499.

[3] M. Elbuluk, N. Langovsky, and D. Kanman, "Design and implementation of a closed-loop observer and adaptive controller for induction motor drives," *IIEEE Trans. Ind. Applicat.*, vol. 34, pp. 435–443, May/June 1998.

[4] F. Peng and T. Fukuo, "Robust speed identification for speed-sensorless vector control of induction motors," *IEEE Trans. Ind. Applicat.*, vol. 30, pp. 1234–1240, Sept./Oct. 1994.

[5] K. Hurst, T. Habetler, G. Griva, and F. Profumo, "Zero-speed tacholess IM torque control: Simply a matter of stator voltage integration," *IEEE Trans. Ind. Applicat.*, vol. 34, pp. 790–794, July/Aug. 1998.

[6] M. Shin, D. Hyun, S. Cho, and S. Choe, "An improved stator flux estimation for speed sensorless stator control of induction motors," *IEEE Trans. Ind. Applicat.*, vol. 15, pp. 312–317, Mar./Apr. 2000.

[7] C. Bonanno, L. Zhen, and L. Xu, "A direct field oriented induction machine drive with robust flux estimator for position sensorless control," presented at the IEEE-IAS Annu. Meeting, Lake Buena Vista, FL, 1995.

[8] H. Kubota, K. Matsuse, and T. Nakano, "DSP-based speed adaptive flux observer of induction motor," *IEEE Trans. Ind. Applicat.*, vol. 29, pp. 344–347, Mar./Apr. 1993.

[9] G. Yang and T. Chin, "Adaptive-speed identification scheme for a vector controlled speed sensorless inverter-induction motor drive," *IEEE Trans. Ind. Applicat.*, vol. 29, pp. 820–825, July/Aug. 1993.

[10] L. Harnefors and H. Nee, "Sensorless control of induction motors for improved low-speed performance," in *Conf. Rec. IEEE-IAS Annu. Meeting*, 1996, pp. 278–285.

[11] H. Kubota, Y. Kataoka, H. Ohta, and K. Matsuse, "Sensorless vector controlled induction machine drives with fast stator voltage offset compansation," in *Conf. Rec. IEEE-IAS Annu. Meeting*, 1999, pp. 2321–2324.

[12] V. I. Utkin, "Sliding mode control design principles and applications to electric drives," *IEEE Trans. Ind. Electron.*, vol. 40, pp. 23–36, Feb. 1993.

[13] S. Doki, S. Sangwongwnich, T. Yonemotor, and S. Okuma, "Implementation of speed-sensorless field-oriented vector control using adaptive sliding observers," in *Proc. IEEE IECON'92*, 1992, pp. 453–458.

[14] F. Parasiliti, R. Petrella, and M. Tursini, "Adaptive sliding-mode observer for speed sensorless control of induction motors," *IEEE Trans. Ind. Applicat.*, vol. 46, pp. 128–137, Jan./Feb. 1999.

[15] V. I. Utkin, *Sliding in Control and Optimization*. Berlin, Germany: Springer-Verlag, 1992.